

Article

## Reaction Kinetic Parameters and Surface Thermodynamic Properties of Cu<sub>2</sub>O Nanocubes

Xingxing Li <sup>1</sup>, Huanfeng Tang <sup>1</sup>, Xianrui Lu <sup>1</sup>, Shi Lin <sup>1</sup>, Lili Shi <sup>1</sup> and Zaiyin Huang <sup>1,2,3,\*</sup>

<sup>1</sup> School of Chemistry and Chemical Engineering, Guangxi University for Nationalities, Nanning, 530008, China

<sup>2</sup> Key Laboratory of Forest Chemistry and Engineering, Guangxi University for Nationalities, Nanning, 530008, China

<sup>3</sup> Guangxi Colleges and Universities Key Laboratory of Food Safety and Pharmaceutical Analytical Chemistry, Guangxi University for Nationalities, Nanning, 530008, China

\* Author to whom correspondence should be addressed; E-Mail: zaiyinhuang@gxun.cn; Tel.: +86-771-3262120; Fax: +86-771-3261718.

Academic Editors: A. Perez-Madrid and Iván Santamaría-Holek

Received: 15 May 2015 / Accepted: 1 July 2015 / Published: 30 July 2015

---

**Abstract:** Cuprous oxide (Cu<sub>2</sub>O) nanocubes were synthesized by reducing Cu(OH)<sub>2</sub> in the presence of sodium citrate at room temperature. The samples were characterized in detail by field-emission scanning electron microscopy, transmission electron microscopy, high-resolution transmission electron microscopy, X-ray powder diffraction, and N<sub>2</sub> absorption (BET specific surface area). The equations for acquiring reaction kinetic parameters and surface thermodynamic properties of Cu<sub>2</sub>O nanocubes were deduced by establishment of the relations between thermodynamic functions of Cu<sub>2</sub>O nanocubes and these of the bulk Cu<sub>2</sub>O. Combined with thermochemical cycle, transition state theory, basic theory of chemical thermodynamics, and *in situ* microcalorimetry, reaction kinetic parameters, specific surface enthalpy, specific surface Gibbs free energy, and specific surface entropy of Cu<sub>2</sub>O nanocubes were successfully determined. We also introduced a universal route for gaining reaction kinetic parameters and surface thermodynamic properties of nanomaterials.

**Keywords:** nanothermodynamics; cuprous oxide; nanocrystal; specific surface enthalpy; specific surface Gibbs free energy; specific surface entropy

---

## 1. Introduction

Surface atomic structure is a critical factor affecting many physical and chemical properties of nanomaterials occurring on its surfaces [1,2], including chemical thermodynamics [3–9], chemical kinetics [5,8], catalysis [10–13], sense [11], adsorption [14], phase transition [15], and electrochemistry of nanomaterials [16]. Surface thermodynamic properties are the intuitive expression of the special structure-activity relationships of nanomaterial surfaces. It is commonly believed that micro/nanocrystals with high-energy facets are known to possess an enhanced reactivity [1,2].

To date, much progress has been made in experimental determination of solid surface energy, including calorimetry for surface enthalpy [17], inert gas bubble precipitation [18], grain boundary grooving kinetics [19], and surface scratch relaxation rate [20] for surface energy, contact angle [21,22], multiphase equilibrium lattice parameters [23], sessile cylinder [19], and zero creep [24] for surface tension. Methods commonly used in Young modulus (e.g., tearing) and other methods involving compression, solubilization, high-temperature dissolution, or lowering of melting point produce high and even applied stress-covered surface energies [25].

Theoretical calculation may be a powerful approach to evaluate surface energies of nanomaterials or their oriented facets [26–28]. However, these methods conducted by theoretical calculations have several limitations [29,30]. Furthermore, most of these employed the ideal models, which were far from reality. Real surfaces with high density of atomic steps, edges, and unsaturated bonds are thermodynamically unstable, which tend to absorb water [7], gas molecules, and surfactants [1,2], undergo surface atom reconstruction and aggregation, or even form a protective film layer. The surface energies of these complicated real surfaces are extremely difficult to theoretically calculate. A universal method to determine surface energy has yet to be developed. Therefore, developing a scientific and universal experimental method to measure the surface energy of nanomaterials is a pressing need in the scientific endeavors on solid surface and in other disciplines.

Cuprous oxide ( $\text{Cu}_2\text{O}$ ) is widely used due to its perspective application in antibacterial activity [31], photocatalysis [32–34], gas sensors [35], chemical templates [36], solar driven water splitting [37,38], CO oxidation [39,40], and catalysis [41]. In terms of studying surface energies of nanoparticles and their structure–function relationship among morphology, structure, and size, there is little literature regarding the theoretical or experimental determination of surface energy of  $\text{Cu}_2\text{O}$  nanocrystals. In this work, cuprous oxide ( $\text{Cu}_2\text{O}$ ) nanocubes were prepared by a facile method via reducing  $\text{Cu}(\text{OH})_2$  in the presence of sodium citrate at room temperature. The equations for acquiring reaction kinetic parameters and surface thermodynamic properties of  $\text{Cu}_2\text{O}$  nanocubes were deduced by establishment of the relations between thermodynamic functions of  $\text{Cu}_2\text{O}$  nanocubes and these of the bulk  $\text{Cu}_2\text{O}$ . Combined with thermochemical cycle, transition state theory, basic theory of chemical thermodynamics, and *in situ* microcalorimetry, reaction kinetic parameters and specific surface energies of  $\text{Cu}_2\text{O}$  nanocubes were successfully determined. We also introduced an universal route for gaining reaction kinetic parameters and surface thermodynamic functions of nanomaterials.

## 2. Results and Discussion

Figure 1a shows that the prepared Cu<sub>2</sub>O nanocubes have a high uniform and monodispersed morphology, enclosed by (100) facets without any truncation. As shown in Figure 1d, the length of its edge is in the range of 46–62 nm. Figure 1b displays the low-magnification TEM image of sample, showing that Cu<sub>2</sub>O nanocubes are highly uniform and have an average size of 55 nm. Visible lattice fringes with d-spacings of 3.04 Å and 2.6 Å are identified in Figure 1c, corresponding to the (110) and (111) lattice planes of Cu<sub>2</sub>O. Figure 1e presents the morphology of bulk Cu<sub>2</sub>O; its size was in the range of 2.9–17.5 μm without any pores in its facets.

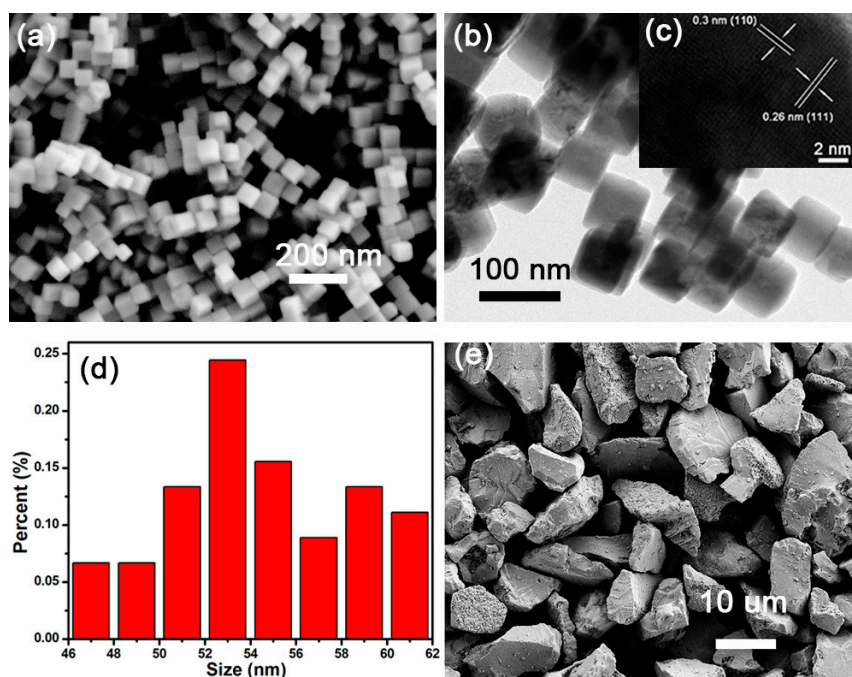


**Figure 1.** SEM images of (a) Cu<sub>2</sub>O nanocubes and (e) bulk Cu<sub>2</sub>O; (b) TEM image of Cu<sub>2</sub>O nanocubes and (c) HR image of tilted nanocube; (d) The size distribution of Cu<sub>2</sub>O nanocubes.

Figure 2a shows that all diffraction peaks of both Cu<sub>2</sub>O nanocubes and bulk Cu<sub>2</sub>O are consistent with those of cuprite cuprous oxide (JCPDF No. 05-0667), no other impurity peak is observed. The sharp diffraction peaks indicate that the samples are highly crystallized. The N<sub>2</sub> absorption-desorption isotherm (Figure 2b) shows that isotherms and hysteresis loops of Cu<sub>2</sub>O nanocubes belong to the typical type IV isotherm and type H3 loop (based on the International Union of Pure and Applied Chemistry (IUPAC) classification), while the N<sub>2</sub> absorption-desorption isotherm of bulk Cu<sub>2</sub>O is almost overlapping, indicating the absence of nonporous macropores on its surface. The specific surface area (BET) of Cu<sub>2</sub>O nanocubes and bulk Cu<sub>2</sub>O are 10.9570 m<sup>2</sup>/g and 0.0106 m<sup>2</sup>/g, respectively.

The reaction heat could be determined by the integration area of heat flow curve (shown in Table 1), and then its molar enthalpies were calculated and exhibited in Table 1.

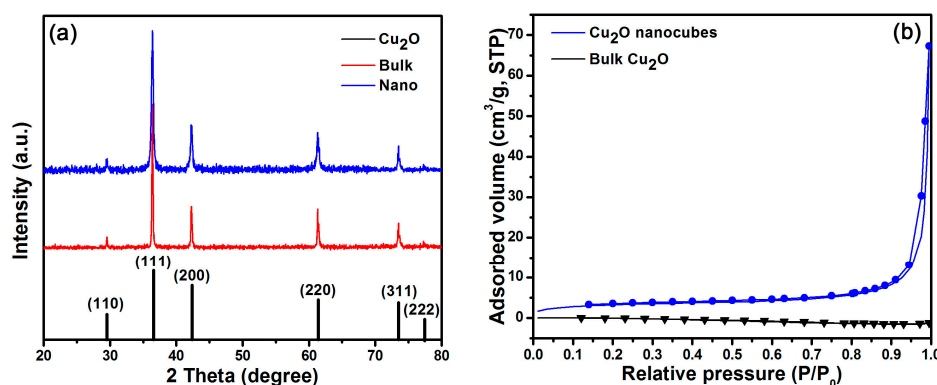


**Figure 2.** (a) X-ray diffraction (XRD) patterns and (b) N<sub>2</sub> absorption-desorption isotherms of nanocubes and bulk Cu<sub>2</sub>O.

**Table 1.** Molar reaction enthalpies of nanocubes and bulk Cu<sub>2</sub>O reaction systems.

T/K	No.	m/mg	Q/J	$\Delta_r H_m^\theta / \text{kJ} \cdot \text{mol}^{-1}$	$\ln k$	
298.15	Nano	1	1.504	2.778	-264.707	-5.544
		2	1.494	2.746	-263.031	-5.565
		3	1.494	2.708	-259.343	-5.550
	Bulk	1.496	2.322	-223.503	-6.153	
303.15	Nano	1	1.503	2.511	-240.575	-5.494
		2	1.501	2.501	-239.914	-5.519
		3	1.496	2.485	-239.198	-5.511
	Bulk	1.500	2.289	-213.421	-5.779	
318.15	Nano	1	1.507	2.078	-198.516	-5.200
		2	1.503	2.066	-197.949	-5.530
		3	1.499	2.069	-198.719	-5.418
	Bulk	1.503	1.808	-173.178	-5.685	

Compared with bulk Cu<sub>2</sub>O, super-refined materials have significantly more particles in the surface phase. Particles in the surface phase account for a large proportion of the total particles. Atoms in the surface phase have uneven stresses, unsaturated force field, and dangling bonds, which lead to high surface energy. This result may explain why the reaction rate of Cu<sub>2</sub>O nanocubes is faster than that of bulk Cu<sub>2</sub>O. With temperature increasing, surface turbulence and surface energy of Cu<sub>2</sub>O nanocubes increase, consequently, resulting in the increase of its chemical reaction rate.

Linear regression of logarithmic reaction rate constant and temperature reciprocal was performed using Equation (6), and the  $E_a$  of the Cu<sub>2</sub>O nanocubes reaction was obtained. The  $\Delta G_{\neq}^\theta$  of the Cu<sub>2</sub>O nanocubes reaction was calculated using Equation (7). The  $\Delta H_{\neq}^\theta$  and  $\Delta S_{\neq}^\theta$  of the Cu<sub>2</sub>O nanocubes reaction were calculated using Equation (8) and shown in Table 2.

Applying Equations (23)–(25), specific surface functions of Cu<sub>2</sub>O nanocubes were determined and shown in Table 3.

Compared with bulk Cu<sub>2</sub>O, specific surface enthalpy, specific surface Gibbs free energy, and specific surface entropy of Cu<sub>2</sub>O nanocube are all larger than these of the bulk. After super-refinement of the material, atoms in surface phase suffer from uneven stress, display unsaturated force field, and possess dangling bonds because of the strong specific surface effect. Consequently, the interaction of

nanoparticles is enhanced, giving rise to the increase of these surface energy with particle size decreasing. This is why nanomaterials have a much higher surface energy than the corresponding bulk materials.

**Table 2.** Activation energy, activation Gibbs free energy, activation enthalpy, and activation entropy of Cu<sub>2</sub>O nanocubes.

Reaction System	<i>T</i> (K)	ln <i>k</i>	$\Delta G_{\ddagger}^0$ (kJ·mol <sup>-1</sup> )	$E_a$ (kJ·mol <sup>-1</sup> )	$\Delta H_{\ddagger}^0$ (kJ·mol <sup>-1</sup> )	$\Delta S_{\ddagger}^0$ (J·K <sup>-1</sup> ·mol <sup>-1</sup> )
Cu <sub>2</sub> O Nanocubes	298.15	-5.553	86.785	6.698	4.134	277.214
	303.15	-5.508	88.169			
	318.15	-5.383	92.323			

**Table 3.** Specific surface functions of Cu<sub>2</sub>O nanocube.

T/K	298.15	303.15	318.15
$H^S$ (J·m <sup>-2</sup> )	24.874	16.611	15.998
$G^S$ (J·m <sup>-2</sup> )	0.943	0.433	0.507
$S^S$ (J·m <sup>-2</sup> ·K <sup>-1</sup> )	0.080	0.053	0.049

### 3. Experimental Section

Copper sulfate (≥ 99%), sodium hydroxide (≥ 99%), trisodium citrate dehydrate (≥ 99%), nitric acid (65–68%), potassium chloride (99.99%), and ascorbic acid (≥ 99.7%) were bought from Sinopharm Chemical Reagent Co. Ltd. and used without further purification. Bulk cuprous oxide (≥ 99%) was gained by physically filtrating the purchased powder from Aladdin Reagent Ltd.. Deionized water used in all experiments had a resistivity of 18.2 MΩ·cm.

The morphologies of the sample were imaged by field-emission scanning electron microscope (FESEM, Zeiss SUPRA 55 Sapphire, Germany). Transmission electron microscopy (TEM) characterization was operated on a JEOL JEM-2100 electron microscope. The X-ray diffraction (XRD) pattern was recorded by X-ray powder diffraction (XRD, Philips PW 1710 with Cu Kα radiation, λ = 1.5406 Å, The Netherlands). The specific surface area was determined by a physisorption analyzer accelerated surface area and porosimetry system (BET, Micromeritics ASAP 2020, USA). The trace amounts of the samples were weighted by an XPE analytic balance (Mettler Toledo, Switzerland). Calorimetric experiments were carried out by a RD496L microcalorimeter (Mianyang CP Thermal Analysis Instrument Co., Ltd, China) under the condition of constant temperature and constant pressure.

In a typical synthesis [40], monodispersed Cu<sub>2</sub>O nanocubes with an average edge length of 55 nm were prepared by reducing Cu(OH)<sub>2</sub> in the presence of sodium citrate which acted as a chelating agent with Cu<sup>2+</sup>, retarding the precipitation of Cu(OH)<sub>2</sub>.

The calorimeter was calibrated by Joule effect and determining the dissolution enthalpy of KCl in deionized water (1:1110, m<sub>KCl</sub>/m<sub>de-water</sub>) at 298.15 K, the result showed that its calorimetric constant and the dissolution enthalpy of KCl were (69.91 ± 0.56) μV·mW<sup>-1</sup> and (17.792 ± 0.029) kJ·mol<sup>-1</sup>, respectively, which was consistent with the value of (17.524 ± 0.028) kJ·mol<sup>-1</sup> in the literature [42], indicating that the microcalorimeter is accurate and reliable.

A small glass tube charged with 1.0 mL of 2.0 M HNO<sub>3</sub> solution was placed above a 15-mL glass tube containing 1.500 mg of Cu<sub>2</sub>O samples (bulk or the obtained nanocubes). After balance of the base line, the upper glass tube charged with HNO<sub>3</sub> solution was pierced. The thermodynamic and kinetic information was recorded by the microcalorimeter.

## 4. Methodology

### 4.1. Establishment of Chemical Reaction Kinetic Models for Nanocubes

Both the specific surface area and specific surface energy of the reactant increase after its size is refined. Thus, the mean molar energy of the refined reactant is higher than that of the corresponding bulk reactant. If the reactant particle size is insignificant to the mean energy of the activated molecules, then the difference between the mean energy of 1 M of activated molecular and 1 M of its reactant is the activation energy of its nanomaterials [7]. Figure 3 shows the transition state theory [7,8]. In the same chemical reaction, the reactant experiences the same transition state to the final state. Therefore, the apparent activation energy of nanoparticles  $E_a$  (nano) is the difference between the activation energy of corresponding bulk materials  $E_a$  (bulk) and the molar surface energy of nanoparticles ( $E_m^S$ ):

$$E_a(\text{nano}) = E_a(\text{bulk}) - E_m^S \quad (1)$$

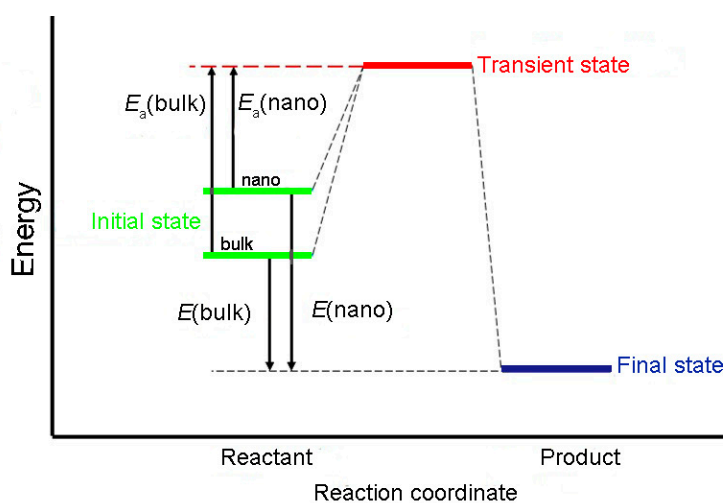


**Figure 3.** Schematic of relationship between surface energy and apparent activation energy.

If the dispersion phase in heterogeneous reaction has only one reactant and others belong to the continuous phase, then the relationship between surface energy and apparent activation energy for nanocubes without inner bores can be expressed as

$$E_a(\text{nano}) = E_a(\text{bulk}) - E_m^S = E_a(\text{bulk}) - \frac{4\sigma M}{\rho l} \quad (2)$$

where  $\sigma$ ,  $M$ ,  $\rho$ , and  $l$  are the surface tension, molar mass, density, and particle size (length of cube edge) of the cubic nanoparticle reactant, respectively. Equation (2) provides that apparent activation energy in chemical reaction of nanomaterials is proportional to the particle size of reactant.

If heterogeneous reaction follows Arrhenius Law, substituting Equation (2) into it yields the Arrhenius equation of nanocubes:

$$k = A \exp\left(-\frac{E_a^b}{RT} + \frac{4\sigma M}{RT\rho l}\right) \quad (3)$$

where  $T$  donates the reaction temperature,  $k$  donates the reaction rate constant,  $A$  donates the pre-exponential factor,  $R$  donates the molar gas constant, and  $E_a^b$  donates the apparent activation energy of corresponding bulk materials.

Substituting the logarithm on both sides of Equation (3), we obtain:

$$\ln k = \ln A - \frac{E_a^b}{RT} + \frac{4\sigma M}{\rho l} \quad (4)$$

therefore, when the particle size is larger than 10 nm, the surface tension slightly changes and can be viewed as a constant [43]. On the basis of Equation (4), the logarithm of the reaction rate constant is inversely proportional to the particle size of the reactant.

#### 4.2. Acquisition of Dynamic Parameters of Cu<sub>2</sub>O Nanocubes Reacting with HNO<sub>3</sub>

The thermodynamic equation of reversible chemical reaction under constant temperature and pressure can be expressed as [44]:

$$\ln\left[\frac{1}{H_\infty} \frac{dH_i}{dt}\right] = \ln k + n \ln\left[1 - \frac{H_i}{H_\infty}\right] \quad (5)$$

where  $H_\infty$  is the enthalpy change during the whole reaction and may be directly obtained by microcalorimetry,  $dH_i/dt$  is the enthalpy change rate,  $k$  (s<sup>-1</sup>) is the reaction rate constant expressed by conversion rate, and  $H_i$  is the enthalpy change at reaction time  $t$ .  $k$  can be calculated from the linear regression of thermodynamic data.

$$\ln k = \ln A - \left[\frac{E_a}{RT}\right] \quad (6)$$

$$\Delta G_\ddagger^\theta = RT \ln\left[\frac{RT}{N_A h k}\right] \quad (7)$$

$$\ln \frac{k}{T} = \ln \frac{k_B}{h} + \frac{\Delta S_\ddagger^\theta}{R} - \frac{\Delta H_\ddagger^\theta}{RT} \quad (8)$$

where  $N_A$  donates Avogadro's constant,  $k_B$  donates Boltzmann's constant,  $h$  donates Planck's constant, and  $R$  donates the molar gas constant;  $\Delta G_\ddagger^\theta$ ,  $\Delta H_\ddagger^\theta$ , and  $\Delta S_\ddagger^\theta$  is activation Gibbs free energy, activation enthalpy, and activation entropy, respectively. The diagram of  $1/T$  was drawn with  $\ln k$ .  $E_a$  and  $A$  were calculated using Equation (6). Activation energies were gained from Equations (7) and (8).

#### 4.3. Theoretical Derivation of Specific Surface Energies

Because of their high specific effects, nanomaterials exhibit more exceptional properties than corresponding bulk materials [1,2]. The specific surface area, specific surface capacity and the specific surface energy should be considered [3]. In a reaction system involving nanoparticles, its overall enthalpy ( $D_r H_m^n$ ) is made of that in bulk portion ( $D_r H_m^b$ ) and in surface/interfacial portion ( $D_r H_m^s$ ) [3–10,43,45], which could be expressed as:

$$D_r H_m^n = D_r H_m^b + D_r H_m^s \quad (9)$$

where n denotes nanosystem, bulk phase is denoted by b, and surface phase is denoted by s.

The essential difference between nano Cu<sub>2</sub>O and bulk Cu<sub>2</sub>O only lies in the size themselves but with the same chemical composition. As shown in Figure 4, the relationship between standard molar enthalpies of formation among them was built via designing a thermochemical cycle [8,9].

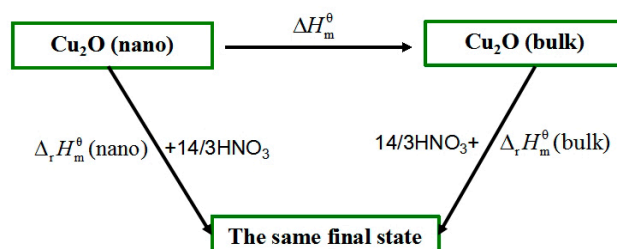
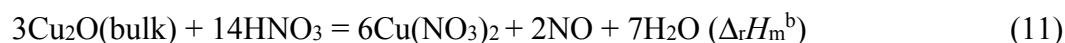
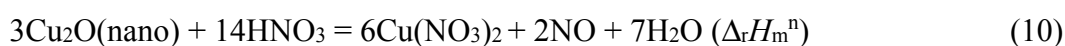


**Figure 4.** Schematic diagram of thermochemical cycle.

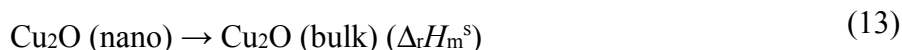
The related reactions in Figure 4 were as follows:



According to the Equation (9),  $\Delta_r H_m^s$  can be expressed as:

$$\Delta_r H_m^s = \Delta_r H_m^n - \Delta_r H_m^b \quad (12)$$

Thus, based on Hess law, the chemical equations for  $\Delta_r H_m^s$  could be deduced by: Reaction (10) and Reaction (11). Therefore, the chemical equation for  $\Delta_r H_m^s$  is as below:



Based on the definition of surface enthalpy of a solid [46], molar surface enthalpy of nanocube Cu<sub>2</sub>O could be deduced by the following chemical equation:



Combining Reaction (13) with Reaction (14), its molar surface enthalpy could be represent as:

$$H_m^s = -\Delta_r H_m^s \quad (15)$$

Coupling Equations (9) and (12) with Equation (15), the molar surface enthalpy of nanocube Cu<sub>2</sub>O could be deduced as:

$$H_m^s = \Delta_r H_m^b - \Delta_r H_m^n \quad (16)$$

Similarly, the molar surface Gibbs free energy of Cu<sub>2</sub>O nanocubes could be derived as:

$$G_m^s = \Delta_r G_m^b - \Delta_r G_m^n \quad (17)$$

It is well known that a chemical reaction occurs on the molecular or atom level. Therefore, the Cu<sub>2</sub>O nanocubes and its corresponding bulk Cu<sub>2</sub>O have the same transition states and final states apart from their initial states [8,9]. The relationship between surface Gibbs free energy and activation Gibbs free energy of the reaction system are presented in Figure 5.

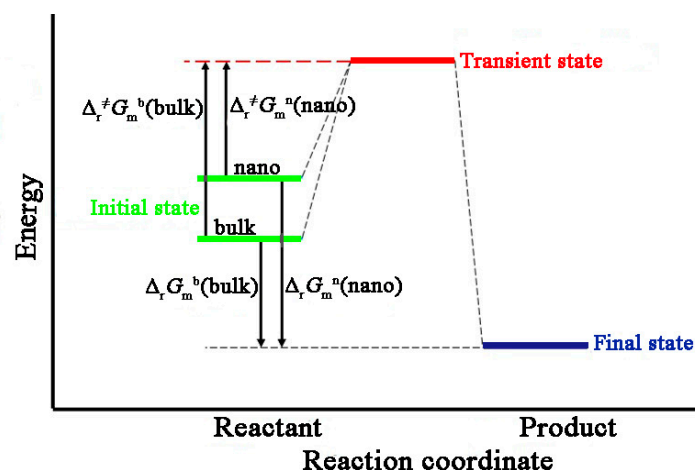


**Figure 5.** Schematic of relationship between surface Gibbs free energy and activation Gibbs free energy.

Therefore, according to characteristics of state function, the following equations can be derived from:

$$\Delta_r G_m^b = \Delta_r^\ddagger G_m^b + \Delta_r G_m \tag{18}$$

$$\Delta_r G_m^n = \Delta_r^\ddagger G_m^n + \Delta_r G_m \tag{19}$$

Combined Equations (17)–(19), molar surface Gibbs free energy of Cu<sub>2</sub>O nanocubes could be deduced by:

$$G_m^s = \Delta_r^\ddagger G_m^b - \Delta_r^\ddagger G_m^n \tag{20}$$

As the transition state theory [46] is shown, the relation between rate constant and Gibbs free energy of activation can be indicated as:

$$k = \frac{k_B T}{h} \exp\left(-\frac{\Delta_r^\ddagger G_m}{RT}\right) \tag{21}$$

where *k<sub>B</sub>* denotes Boltzmann constant, and *h* denotes Planck constant.

Combined with the Equations (20) and (21), *G<sub>m</sub><sup>s</sup>* can be transferred as:

$$G_m^s = RT (\ln k_{\text{nano}} - \ln k_{\text{bulk}}) \tag{22}$$

Based on the fundamental definition of thermodynamic function, the specific surface enthalpy and specific surface Gibbs free energy of nanomaterials was expressed [8]:

$$H^s = \frac{-\Delta_r H_m^s}{M(A_{\text{nano}} - A_{\text{bulk}})} \tag{23}$$

$$G^s = \frac{-\Delta_r G_m^s}{M(A_{\text{nano}} - A_{\text{bulk}})} \tag{24}$$

where *M* and *A* represent molar mass and surface area determined by BET, *H<sup>s</sup>* is the enthalpy per unit area, *G<sup>s</sup>* is the surface Gibbs free energy per unit area.

In accordance with the formula *G<sup>s</sup> = H<sup>s</sup> - TS<sup>s</sup>*, the, and the specific surface entropy *S<sup>s</sup>* of Cu<sub>2</sub>O nanocubes can be gained as:

$$S^s = (H^s - G^s)/T \tag{25}$$

where  $S^s$  is the surface entropy per unit area.

## 5. Conclusions

Cuprous oxide ( $\text{Cu}_2\text{O}$ ) nanocubes were prepared by reducing  $\text{Cu}(\text{OH})_2$  in the presence of sodium citrate, which acted as a chelating agent with  $\text{Cu}^{2+}$  at room temperature. In addition, the samples were characterized in detail by field-emission scanning electron microscopy, transmission electron microscopy, high-resolution transmission electron microscopy, X-ray powder diffraction, and  $\text{N}_2$  absorption (BET specific surface area). The equations for acquiring reaction kinetic parameters and surface thermodynamic properties of  $\text{Cu}_2\text{O}$  nanocubes were deduced by establishment of the relations between thermodynamic functions of  $\text{Cu}_2\text{O}$  nanocubes and these of the bulk  $\text{Cu}_2\text{O}$ . Then thermochemical cycle combined with transition state theory, basic theory of chemical thermodynamics, and *in situ* microcalorimetry, reaction kinetic parameters, specific surface enthalpy, specific surface Gibbs free energy, and specific surface entropy of  $\text{Cu}_2\text{O}$  nanocubes were successfully determined. We also introduced a universal route for gaining reaction kinetic parameters and surface thermodynamic properties of nanomaterials.

## Acknowledgments

The authors would like to thank the Natural Science Foundation of China (20963001, 21273050) for their financial support. They also express their great appreciation to Guangxi Colleges and Universities Key Laboratory of Food Safety and Pharmaceutical Analytical Chemistry (Guangxi University for Nationalities) and Xuecai Tan for professional language services.

## Author Contributions

Zaiyin Huang conceived the idea; Xingxing Li did the detailed experimental program, data processing, and wrote the article; Huangfeng Tang did the calorimetric experiment; Xianrui Lu, Shi Lin, and Lili Shi synthesized  $\text{Cu}_2\text{O}$  nanocubes; All authors have read and approved the final manuscript.

## Conflicts of Interest

The authors declare no conflict of interest.

## References

1. Zhou, Z.Y.; Tian, N.; Li, J.T.; Broadwell, I.; Sun, S.G. Nanomaterials of High Surface Energy with Exceptional Properties in Catalysis and Energy Storage. *Chem. Soc. Rev.* **2011**, *40*, 4167–4185.
2. Kuang, Q.; Wang, X.; Jiang, Z.; Xie, Z.; Zheng, L. High-Energy-Surface Engineered Metal Oxide Micro and Nanocrystallites and Their Applications. *Account. Chem. Res.* **2013**, *47*, 308–318.
3. Xue, Y.Q.; Gao, B.J.; Gao, J.F. The Theory of Thermodynamics for Chemical Reactions in Dispersed Heterogeneous Systems. *J. Colloid Interface Sci.* **1997**, *191*, 81–85.

4. Du, J.; Zhao, R.; Xue, Y.Q. Effects of Sizes of Nano-copper Oxide on the Equilibrium Constant and Thermodynamic Properties for the Reaction in Nanosystem. *J. Chem. Thermodyn.* **2012**, *45*, 48–52.
5. Du, J.P.; Wang, H.Y.; Zhao, R.H. Size-dependent Thermodynamic Properties and Equilibrium Constant of Chemical Reaction in Nanosystem: An Experimental Study (II). *J. Chem. Thermodyn.* **2013**, *65*, 29–33.
6. Mazeina, L.; Deore, S.; Navrotsky, A. Energetics of Bulk and Nano-akaganeite,  $\beta$ -FeOOH: Enthalpy of Formation, Surface Enthalpy, and Enthalpy of Water Adsorption. *Chem. Mater.* **2006**, *18*, 1830–1838.
7. Mazeina, L.; Deore, S.; Navrotsky, A. Enthalpy of Water Adsorption and Surface Enthalpy of Goethite ( $\alpha$ -FeOOH) and Hematite ( $\alpha$ -Fe<sub>2</sub>O<sub>3</sub>). *Chem. Mater.* **2007**, *19*, 825–833.
8. Li, X.X.; Huang, Z.Y.; Zhong, L.Y.; Wang, T.H.; Tan, X.C. Size Effect on Reaction Kinetics and Surface Thermodynamic Properties of Nano-octahedral Cadmium Molybdate. *Chin. Sci. Bull.* **2014**, *59*, 2490–2498.
9. Li, X.X.; Fan, G.C.; Huang, Z.Y. Synthesis and Surface Thermodynamic Functions of CaMoO<sub>4</sub> Nanocakes. *Entropy* **2015**, *17*, 2741–2748.
10. Fernández-Cañoto, D.; Larese, J.Z. Thermodynamic and Modeling study of Thin n-Heptane Films Adsorbed on Magnesium Oxide (100) Surfaces. *J. Phys. Chem. C* **2014**, *118*, 3451–3458.
11. Hu, L.H.; Peng, Q.; Li, Y. Selective Synthesis of Co<sub>3</sub>O<sub>4</sub> Nanocrystal with Different Shape and Crystal Plane Effect on Catalytic Property for Methane Combustion. *J. Am. Chem. Soc.* **2008**, *130*, 16136–16137.
12. Wen, Y.Z.; Xue, Y.Q.; Cui, Z.X.; Wang, Y. Thermodynamics of Nano-adsorption FROM Solution: Theoretical and Experimental Research. *J. Chem. Thermodyn.* **2015**, *80*, 112–118.
13. Cui, Z.X.; Zhao, M.Z.; Lai, W.P.; Xue, Y.Q. Thermodynamics of Size Effect on Phase Transition Temperatures of Dispersed Phases. *J. Phys. Chem. C* **2011**, *115*, 22796–22803.
14. Yang, Y.F.; Xue, Y.Q.; Cui, Z.X.; Zhao, M.Z. Effect of Particle Size on Electrode Potential and Thermodynamics of Nanoparticles Electrode in Theory and Experiment. *Electrochimica Acta* **2014**, *136*, 565–571.
15. Lipsett, S.G.; Johnson, F.M.; Maas O. The Surface Energy and the Heat of Solution of Solid Sodium Chloride. *J. Am. Chem. Soc.* **1927**, *49*, 925–943.
16. Vargha-Butler, E.I.; Zubovits, T.K.; Hamza, H.A.; Neumann, A.W. Surface Tension Effects in the Sedimentation of Polymer Particles in Various Liquid Mixtures. *J. Dispers. Sci. Technol.* **1985**, *6*, 357–379.
17. Barnes, R.S.; Redding, G.B. The Behavior of Helium Atoms Injected into Beryllium. *J. Nucl. Energy* **1959**, *10*, 32–35.
18. Maiya, P.S.; Blakely, J.M. Surface Self-Diffusion and Surface Energy of Nickel. *J. Appl. Phys.* **1967**, *38*, 698–704.
19. Kendall, K.; Alford, N.M.N.; Birchall, J.D. A New Method for Measuring the Surface Energy of Solids. *Nature* **1987**, *325*, 794–796.
20. Chaudhury, M.K.; Whitesides, G.M. Correlation between Surface Free Energy and Surface Constitution. *Science* **1992**, *255*, 1230–1232. Available online: [http://www.lehigh.edu/mkc4/public/www-data/our%20papers/Chaudhury\\_surface%20energy\\_science.pdf](http://www.lehigh.edu/mkc4/public/www-data/our%20papers/Chaudhury_surface%20energy_science.pdf) (accessed on 28 July 2015).

21. Vermaak, J.S.; Mays, C.W.; Kuhlmann-Wilsdorf D. On Surface Stress and Surface Tension. I. Theoretical Considerations. *Surf. Sci.* **1968**, *12*, 128–133.
22. Rice, C.M.; Eppelsheimer, D.S.; McNeil, M.B. Surface Tension of Solid Tin. *J. Appl. Phys.* **1966**, *37*, 4766–4768.
23. Kumikov, V.; Khokonov, K.B. On the Measurement of Surface Free Energy and Surface Tension of Solid Metals. *J. Appl. Phys.* **1983**, *54*, 1346–1350.
24. Lazzeri, M.; Vittadini, A.; Selloni, A. Structure and Energetics of Stoichiometric TiO<sub>2</sub> Anatase Surfaces. *Phys. Rev. B* **2001**, *63*, 155409.
25. Lazzeri, M.; Vittadini, A.; Selloni, A. Erratum: Structure and Energetics of Stoichiometric TiO<sub>2</sub> Anatase Surfaces. *Phys. Rev. B* **2002**, *65*, 119901.
26. McHale, J.M.; Auroux, A.; Perrotta, A.J.; Navrotsky, A. Surface Energies and Thermodynamic Phase Stability in Nanocrystalline Alumina. *Science* **1997**, *277*, 788–791.
27. Slater, B.; Catlow, C.R.A.; Gay, D.H.; Williams, D.E.; Dusastre, V. Study of Surface Segregation of Antimony on SnO<sub>2</sub> Surfaces by Computer Simulation Techniques. *J. Phys. Chem. B* **1999**, *103*, 10644–10650.
28. Groß, A. The Virtual Chemistry Lab for Reactions at Surfaces: Is it Possible? Will it be Useful? *Surf. Sci.* **2002**, *500*, 347–367.
29. Jardine, A.P.; Dworski, S.; Fouquet, P.; Alexandrowicz, G.; Riley, D.J.; Lee, G.Y.; Allison, W. Ultrahigh-Resolution Spin-echo Measurement of Surface Potential Energy Landscapes. *Science* **2004**, *304*, 1790–1793.
30. Pang, H.; Gao, F.; Lu, Q. Morphology Effect on Antibacterial Activity of Cuprous Oxide. *Chem. Commun.* **2009**, *9*, 1076–1078.
31. Zhang, H.; Zhu, Q.; Zhang, Y.; Wang, Y.; Zhao, L.; Yu, B. One-Pot Synthesis and Hierarchical Assembly of Hollow Cu<sub>2</sub>O Microspheres with Nanocrystals-Composed Porous Multishell and Their Gas-Sensing Properties. *Adv. Funct. Mater.* **2007**, *17*, 2766–2771.
32. Huang, W.C.; Lyu, L.M.; Yang, Y.C.; Huang, M.H. Synthesis of Cu<sub>2</sub>O Nanocrystals from Cubic to Rhombic Dodecahedral Structures and Their Comparative Photocatalytic Activity. *J. Am. Chem. Soc.* **2011**, *134*, 1261–1267.
33. Huang, M.H.; Rej, S.; Hsu, S.C. Facet-Dependent Properties of Polyhedral Nanocrystals. *Chem. Commun.* **2014**, *50*, 1634–1644.
34. Wang, Z.; Luan, D.; Li, C.M.; Su, F.; Madhavi, S.; Boey, F.Y.C.; Lou, X.W. Engineering Nonspherical Hollow Structures with Complex Interiors by Template-Engaged Redox Etching. *J. Am. Chem. Soc.* **2010**, *132*, 16271–16277.
35. Kondo, J. Cu<sub>2</sub>O as a Photocatalyst for Overall Water Splitting under Visible Light Irradiation. *Chem. Commun.* **1998**, *3*, 357–358.
36. Paracchino, A.; Laporte, V.; Sivula, K.; Grätzel, M.; Thimsen, E. Highly Active Oxide Photocathode for Photoelectrochemical Water Reduction. *Nat. Mater.* **2011**, *10*, 456–461.
37. Leng, M.; Liu, M.; Zhang, Y.; Wang, Z.; Yu, C.; Yang, X.; Wang, C. Polyhedral 50-Facet Cu<sub>2</sub>O Microcrystals Partially Enclosed by {311} High-Index Planes: Synthesis and Enhanced Catalytic CO Oxidation Activity. *J. Am. Chem. Soc.* **2010**, *132*, 17084–17087.

38. Wang, X.; Liu, C.; Zheng, B.; Jiang, Y.; Zhang, L.; Xie, Z.; Zheng, L. Controlled Synthesis of Concave Cu<sub>2</sub>O Microcrystals Enclosed by {hhl} High-Index Facets and Enhanced Catalytic Activity. *J. Mater. Chem. A* **2013**, *1*, 282–287.
39. Sun, S.; Yang, Z. Cu<sub>2</sub>O-templated Strategy for Synthesis of Definable Hollow Architectures. *Chem. Commun.* **2014**, *50*, 7403–7415.
40. Chang, I.C.; Chen, P.C.; Tsai, M.C.; Chen, T.T.; Yang, M.H.; Chiu, H.T.; Lee, C.Y. Large-Scale Synthesis of Uniform Cu<sub>2</sub>O Nanocubes with Tunable Sizes by In-situ Nucleation. *CrystEngComm* **2013**, *15*, 2363–2366.
41. Tsai, Y.H.; Chanda, K.; Chu, Y.T.; Chiu, C.Y.; Huang, M.H. Direct Formation of Small Cu<sub>2</sub>O Nanocubes, Octahedra, and Octapods for Efficient Synthesis of Triazoles. *Nanoscale* **2014**, *6*, 8704–8709.
42. Rychlý, R.; Pekarek, V. The Use of Potassium Chloride and Tris (Hydroxymethyl) Aminomethane as Standard Substances for Solution Calorimetry. *J. Chem. Thermodyn.* **1977**, *9*, 391–396.
43. Xue, Y.Q; Effects of Particle Size on Phase Transitions and Reactions of Nanosystems. Ph. D Thesis, Taiyuan University of Technology, Taiyuan, Shanxi, China, 2005.
44. Hu, R.Z.; Zhao, Q.F.; Gao, H.X. *Fundamentals and Application of Calorimetry*; Science Press: Beijing, China, 2011.
45. Radha, A.V.; Bomati-Miguel, O.; Ushakov, S.V.; Navrotsky, A.; Tartaj, P. Surface Enthalpy, Enthalpy of Water Adsorption, and Phase Stability in Nanocrystalline Monoclinic Zirconia. *J. Am. Ceram. Soc.* **2009**, *92*, 133–140.
46. Fu, X.C.; Shen, W.X.; Yao, T.Y.; Hou, W.H. *Physical Chemistry*, 5th ed.; Higher Education Press: Beijing, China, 2006.

© 2015 by the authors; licensee MDPI, Basel, Switzerland. This article is an open access article distributed under the terms and conditions of the Creative Commons Attribution license (<http://creativecommons.org/licenses/by/4.0/>).